CHARACTERIZATION OF THE RUBYS INN THRUST FAULT IN GARFIELD COUNTY, UTAH, USING ELECTRICAL RESISTIVITY TOMOGRAPHY AND TRANSIENT ELECTROMAGNETIC SURVEYS

by Trevor H. Schlossnagle and Kayla D. Smith

REPORT OF INVESTIGATION 290
UTAH GEOLOGICAL SURVEY
UTAH DEPARTMENT OF NATURAL RESOURCES
2025

Blank pages are intentional for printing purposes.

CHARACTERIZATION OF THE RUBYS INN THRUST FAULT IN GARFIELD COUNTY, UTAH, USING ELECTRICAL RESISTIVITY TOMOGRAPHY AND TRANSIENT ELECTROMAGNETIC SURVEYS

by Trevor H. Schlossnagle and Kayla D. Smith

Cover photo: View to the west of Claron-over-Claron fault exposure of the Rubys Inn thrust fault north of Highway 12 in Bryce Canyon National Park.

Suggested citation:

Schlossnagle, T.H., and Smith, K.D., 2025, Characterization of the Rubys Inn thrust fault in Garfield County, Utah, using electrical resistivity tomography and transient electromagnetic surveys: Utah Geological Survey Report of Investigation 290, 19 p., 4 appendices, https://doi.org/10.34191/RI-290.

REPORT OF INVESTIGATION 290
UTAH GEOLOGICAL SURVEY
UTAH DEPARTMENT OF NATURAL RESOURCES
2025

STATE OF UTAH
Spencer J. Cox, Governor

DEPARTMENT OF NATURAL RESOURCES
Joel Ferry, Executive Director

UTAH GEOLOGICAL SURVEY
L. Darlene Batatian, Director

PUBLICATIONS
contact
Natural Resources Map & Bookstore
1594 W. North Temple
Salt Lake City, UT 84116
telephone: 801-537-3320
toll-free: 1-888-UTAH MAP
website: utahmapstore.com
email: geostore@utah.gov

UTAH GEOLOGICAL SURVEY
contact
1594 W. North Temple, Suite 3110
Salt Lake City, UT 84116
telephone: 801-537-3300
website: geology.utah.gov

CONTENTS

FIGURES

TABLE

CHARACTERIZATION OF THE RUBYS INN THRUST FAULT IN GARFIELD COUNTY, UTAH, USING ELECTRICAL RESISTIVITY TOMOGRAPHY AND TRANSIENT ELECTROMAGNETIC SURVEYS

by Trevor H. Schlossnagle and Kayla D. Smith

ABSTRACT

Recent development pressures near Bryce Canyon National Park, Garfield County, Utah, could affect groundwater usage, availability, and dependent resources. A significant fault, the Rubys Inn thrust fault, lies between commonly targeted aquifers in Emery Valley and groundwater of the Paunsaugunt Plateau. In cooperation with the National Park Service, the Utah Geological Survey conducted a geophysical study targeting the Rubys Inn thrust fault, along the southern boundary of Emery Valley. Fault zone geometry and internal structure is typically complex, resulting in heterogeneous permeability distribution which can affect local and regional groundwater flow. The influence of fault zones on groundwater flow parallel and perpendicular to their planes is, therefore, difficult to predict. Geophysical imaging methods can yield important information about subsurface fault geometry.

We combined electrical resistivity tomography (ERT) and transient electromagnetic (TEM) surveys to investigate the field-scale influence of the Rubys Inn thrust fault on groundwater location and movement along the southeast boundary of Emery Valley. We collected ERT and TEM data along three transects roughly orthogonal to the mapped fault strike in May/June 2022 and again in September 2022. These data and existing water-level and lithologic data were used to construct a series of geophysical models that constrain subsurface fault characteristics.

Geophysical models illustrate the complexity and variability of the Rubys Inn thrust fault within a relatively short distance along strike. Model results indicate that where the fault is concealed, the actual location differs from the mapped location by 70 to 100 meters along our transects. Groundwater is well constrained in the fault zone hanging wall but poorly constrained in the footwall, and little seasonal variation is discernible in the data. However, variable stratigraphy and structural features are apparent in all transects. Without better geologic and hydrologic constraints in the footwall, the results of this study do not indicate whether the fault acts as a groundwater flow barrier. Further study is needed to constrain the location of groundwater in and adjacent to the fault zone and understand the movement of groundwater relative to the fault plane.

INTRODUCTION

Groundwater resource development and the threat of future drought in Garfield County, south-central Utah, has prompted recent studies of groundwater in Bryce Canyon National Park and adjacent areas (Wallace and Schlossnagle, 2021; Wallace et al., 2024). Emery Valley, situated predominantly north of Bryce Canyon National Park, is subject to a potential increase in growth from tourism-related development (Figure 1). It is currently uncertain whether groundwater withdrawals in Emery Valley could affect groundwater resources up-gradient in adjoining areas of the Paunsaugunt Plateau and Bryce Canyon National Park.

The Rubys Inn thrust fault is an east-west-striking thrust fault that lies between commonly targeted aquifers in Emery Valley and groundwater flow systems that support springs, seeps, and dependent ecosystems to the south on the Paunsaugunt Plateau. We designed this study to improve our understanding of how the Rubys Inn fault influences groundwater movement between the Paunsaugunt Plateau and Emery Valley. This research allows government agencies and land managers to make science-based water rights and resource management decisions.

Purpose and Scope

The overall goal of this study is to improve the understanding of the hydrogeologic, structural, and stratigraphic characteristics of the Rubys Inn fault. Fault zones have heterogeneous permeability and anisotropy, meaning faults can be both flow barriers and flow conduits (Caine et al., 1996; Bense et al., 2013). We describe the results of three electrical resistivity tomography (ERT) transects and three transient electromagnetic (TEM) transects across the Rubys Inn fault near Bryce Canyon City. We also use groundwater-level data and literature- and field-based outcrop observations of the thrust fault to assist with our interpretations of geophysical models. These data help determine if the Rubys Inn fault acts as a barrier or conduit to cross-fault groundwater flow and therefore the likelihood that Emery Valley development might impact groundwater-dependent resources across the fault. Our results will also help identify suitable locations for future monitoring wells that would enable further investigation of the fault's hydrogeologic control and long-term groundwater monitoring.

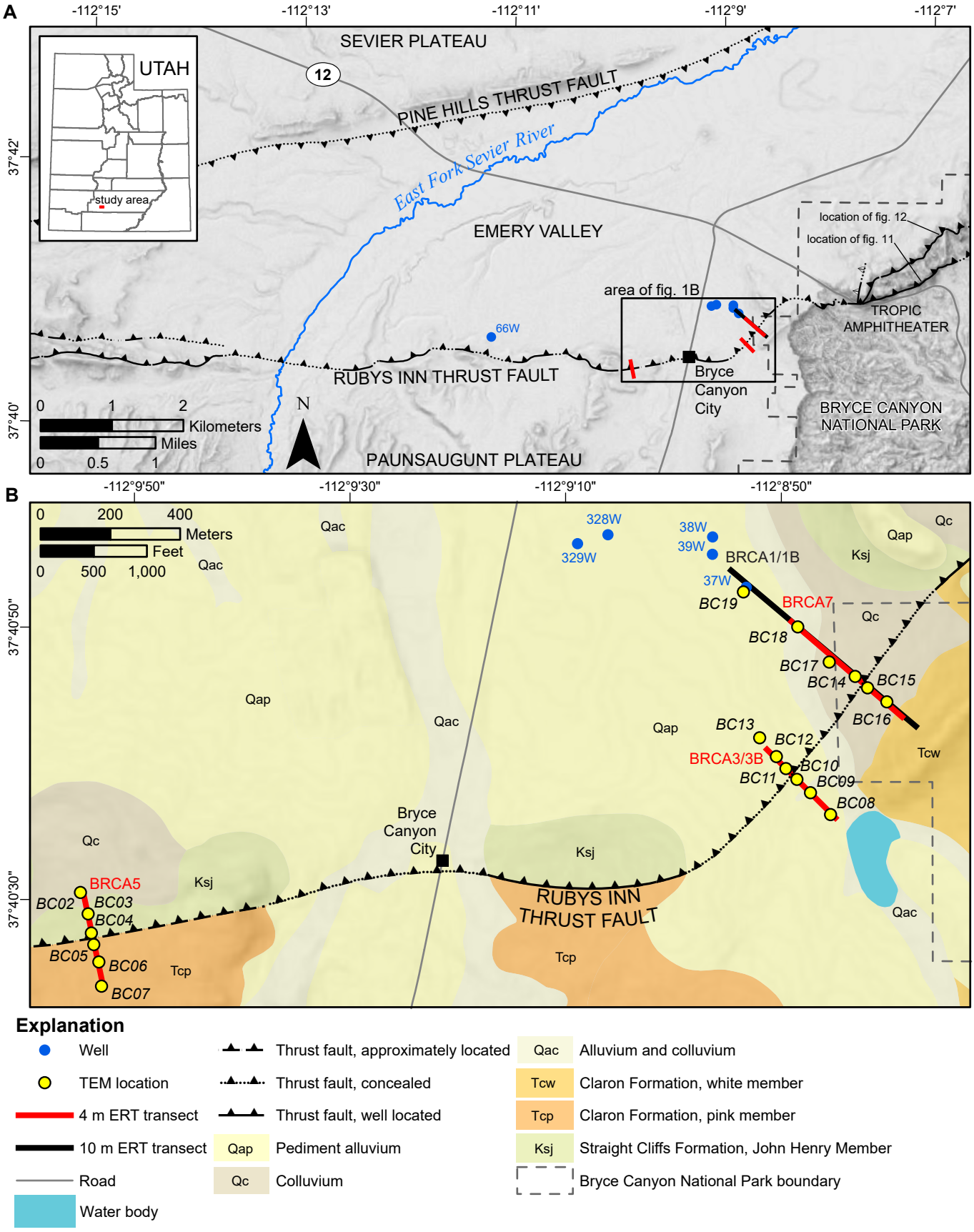

Figure 1. *Shaded-relief maps showing* ***A)*** *location of Emery Valley relative to the Paunsaugunt Plateau and Bryce Canyon National Park and* ***B)*** *study area. Fault locations, 4-m and 10-m electrode spacing electrical resistivity tomography (ERT) transects, transient electromagnetic (TEM) locations, and wells with hydrogeologic data are shown on both maps. Geologic units modified from Biek et al. (2015) are shown on B. Well IDs are consistent with Wallace et al. (2024) and correlate with Table 1.*

STUDY AREA

Location and Geography

The study area is located near Bryce Canyon City, Garfield County, Utah (Figure 1). The area includes the southeast corner of Emery Valley, parts of Bryce Canyon City, and the northwest corner of Bryce Canyon National Park.

Emery Valley is in the High Plateaus subprovince of the Colorado Plateau, also known as the transition zone between the Basin and Range Province to the west and Colorado Plateau Province to the east (Davis, 1999). This structural and stratigraphic transition zone is defined by a series of north-south-striking, west-side-down oblique-slip normal faults.

Emery Valley is a shallow intermontane basin bounded by the Sevier Plateau to the north and the Paunsaugunt Plateau to the south. The Paunsaugunt Plateau is the main recharge area for both Emery Valley and Bryce Canyon National Park, supplying surface water to the East Fork Sevier River and groundwater to Emery Valley and Bryce Canyon National Park.

Geologic Setting

The stratigraphy in the study area consists of Upper Cretaceous to Eocene sedimentary rocks, and Quaternary surficial deposits (Figure 2). The John Henry Member of the Straight Cliffs Formation (Upper Cretaceous) consists of mudstone and fine-grained subarkosic sandstone, that is 240 to 335 meters (m) (800–1100 feet [ft]) thick in Bryce Canyon National Park (Bowers, 1990). The Drip Tank Member of the Straight Cliffs Formation (Upper Cretaceous) consists of fine- to medium-grained quartzose sandstone and pebbly sandstone/conglomerate that ranges from 30 to 60 m (100–200 ft) thick on the Paunsaugunt Plateau (Biek et al., 2015). The Wahweap Formation (Upper Cretaceous) consists of mudstone, fine-grained sandstone, and silty sandstone and thickens east to west on the Paunsaugunt Plateau from around 90 m (300 ft) to 210 m (700 ft), respectively (Lawton et al., 2003). The Kaiparowits Formation (Upper Cretaceous) consists of fine-grained sandstone, mudstone, and siltstone, and is generally locally eroded along the eastern section of the Rubys Inn fault. The pink member of the Claron Formation (Paleocene to Eocene) consists of micritic limestone, calcite-cemented sandstone, and calcareous mudstone

System	Series	Formation or Member	Lithology & weathering profile
Quaternary	Holocene & Pleistocene	Surficial deposits	sand and gravel
Tertiary	Eocene	Conglomerate at Boat Mesa	conglomerate
		Claron Formation; white member	mudstone and micritic limestone
		Claron Formation; pink member	mudstone, siltstone, sandstone, and limestone
	Paleocene		
Cretaceous	Upper	Kaiparowits Formation	sandstone, siltstone, and mudstone
		Wahweap Formation	sandstone, conglomerate, mudstone, and siltstone
		Straight Cliffs Formation; Drip Tank Member	conglomerate and sandstone
		Straight Cliffs Formation; John Henry Member	sandstone, mudstone, and siltstone

Figure 2. *Generalized stratigraphic column showing age and lithology of formations in study area, modified from Biek et al. (2015).*

and is around 180 m (600 ft) thick in Bryce Canyon National Park (Biek et al., 2015). The white member of the Claron Formation (Eocene) typically consists of white micritic limestone but grades to interbedded mudstone, siltstone, and limestone in the northern part of Bryce Canyon National Park (Biek et al., 2015). Changes in lithology within the Claron can be attributed to both depositional environment and bioturbation, the latter of which can cause dramatic lateral changes. The conglomerate at Boat Mesa (Eocene) consists of pebbly conglomerate, calcareous and conglomeratic sandstone, and minor siltstone and mudstone that ranges up to 30 m (100 ft) thick in Bryce Canyon National Park (Bowers, 1990). Quaternary unconsolidated deposits in the study area consist of colluvium and alluvium composed of poorly to moderately sorted clay- to boulder-size sediments deposited by slope-wash, debris flow, soil creep, and ephemeral fluvial processes.

The Rubys Inn fault is part of the Paunsaugunt thrust fault system, a grouping of Middle Tertiary thrust faults that strike perpendicular to the predominant Sevier and Laramide orogenic faulting in the region. This fault system may have resulted in part from the Markagunt gravity slide, formed during Tertiary time due to gravitational collapse of the southern part of the Marysvale volcanic field (Merle et al., 1993; Biek et al., 2015).

The Rubys Inn fault is the most prominent of several south-directed, shallow thrust faults that have a total offset of up to 460 to 910 m (1500–3000 ft) (Lundin, 1989; Davis, 1999). The Rubys Inn fault strikes westward from the Paunsaugunt fault zone, where the surface trace is lost at the western edge of the Paunsaugunt Plateau. However, recent research suggests that the fault continues into the Markagunt Plateau to the west as a blind thrust (Biek et al., 2015). In the study area, the fault places the John Henry Member of the Straight Cliffs Formation over the pink and white members of the Claron Formation. To the east, the fault places Wahweap Formation over the white Claron, and continuing east, pink Claron on top of itself.

Previous Work

Two recent studies examined groundwater in Emery Valley in detail (Wallace and Schlossnagle, 2021; Wallace et al., 2024). Wallace et al. (2024) conducted a comprehensive study on the aquifers of Emery Valley and neighboring Johns Valley to the northeast, as well as groundwater to the south on the Paunsaugunt Plateau and in Bryce Canyon National Park. Their study includes a hydrogeologic framework, a groundwater age analysis, and a water budget. Our current study was motivated by their observation that faults, primarily the Rubys Inn fault and Paunsaugunt fault zone, likely play a role in the groundwater system.

The Rubys Inn fault was identified in the mid-1950s but remained undocumented until 1986 and has since been studied for the following four decades (Biek et al., 2015). Davis and Krantz (1986) discovered evidence of the Paunsaugunt thrust fault system in Bryce Canyon National Park. Lundin (1989) mapped the Rubys Inn fault in detail. Nickelsen and Merle (1991), Nickelsen et al. (1992), Davis (1999), Leavitt et al. (2011), May et al. (2011), and Cleveland et al. (2014) extensively documented compressional deformation in and around the Rubys Inn fault. Although the Rubys Inn fault has been studied extensively, no studies have truly addressed groundwater flow relative to the fault.

METHODS

We used geophysical surveys, hydrogeologic data, and geologic observations to better understand the hydrogeology and structural variability of the Rubys Inn fault. We applied electrical resistivity tomography (ERT) and transient electromagnetics (TEM) to collect subsurface data, create inversion models, and facilitate structural and hydrogeologic interpretations. Used in conjunction, these complementary methods provide high-resolution data to resolve complex structure and stratigraphy at varying depths. ERT and TEM surveys were conducted in May/June and September 2022, the timing of which was intended to capture conditions reflecting presumed maximum and minimum groundwater levels, respectively. We also collected water-level data and compiled lithologic logs and historical water-level data to assist in interpretation of inversion model results.

Hydrogeology

For this study we compiled lithologic logs and historical water-level data from six monitoring wells in the study area (Figure 1, Table 1; Utah Division of Water Rights, 2022; U.S. Geological

Table 1. *Well data in the study area.*

UGS site ID	USGS site ID	Latitude	Longitude	Well Depth (m)	Depth to Bedrock (m)	Depth to water (m)		
						June 1981[1]	June 2022	September 2022
37W	374053112085201	37.681362	-112.148115	44.2	9.1	2.6	3.5	3.8
38W	374054112085701	37.682387	-112.148981	44.2	16.8	4.1	5.0	5.2
39W	374053112085701	37.682033	-112.148986	44.2	9.1	4.1	5.1	5.2
66W	374032112103301	37.677285	-112.186335	15.2	-	2.1	-	-
328W	374054112090501	37.682438	-112.151689	59.4	21.3	6.4	7.3	7.5
329W	374053112090701	37.682256	-112.152472	50.3	18.3	6.3	7.2	7.4

[1] Data from U.S. Geological Survey National Water Information System database NAD83 coordinate reference system

Survey, 2023). We measured water levels from five of these wells (excluding well 66W) during both the May/June and September 2022 geophysical data collection periods.

ERT Survey

ERT is an active-source, subsurface imaging technique that uses a series of electrodes to produce currents and measure electrical potentials along user-designed transects. The measured electrical potentials, or voltage differences, depend on the distribution of electrical resistivity in the subsurface and the geometry of the electrode layout. For a detailed description of ERT methodologies, refer to Johnson et al. (2010), Singha et al. (2014), and Binley and Slater (2020). Electrical resistivity in the subsurface varies with lithologic and hydrologic conditions, including degree of saturation, porosity, fracturing, pore fluid salinity, and mineral composition (Archie, 1942; Zohdy et al., 1974; Palacky, 1988; Nabighian and Macnae, 1991). ERT has been widely used for investigating faults for the past two decades (e.g., Suzuki et al., 2000; Wise et al., 2003; Caputo et al., 2007; Ball et al., 2010; Saribudak and Hawkins, 2019; Barnes et al., 2021).

We conducted all ERT surveys with an Advanced Geosciences Incorporated (AGI) SuperSting™ Wi-Fi R8 electrical resistivity meter and 56-electrode passive cabling system (Figure 3). We surveyed three two-dimensional (2D) ERT transects centered on and roughly orthogonal to the Rubys Inn fault as mapped by Biek et al. (2015) from May 17 to May 19, 2022. One 550-m transect was measured with 10-m electrode spacing (BRCA1) and two 220-m transects with 4-m electrode spacing (BRCA3 and BRCA5) (Figure 1). From September 13 to September 15, 2022, we repeated the 10-m electrode spacing survey (BRCA1B) and central 4-m electrode spacing survey (BRCA3B) and performed a higher resolution 332-m length 4-m electrode spacing survey along a portion of BRCA1 (BRCA7). Survey BRCA7 was collected "roll-along" style, meaning overlapping data were collected to generate a longer survey line using a shorter electrode spacing to achieve higher resolution over a greater area. Each survey was executed with a hybrid dipole-dipole/strong-gradient array developed and recommended by AGI (AGI, 2020). The dipole-dipole component provides high-resolution data whereas the strong-gradient component provides higher signal levels. Maximum depth of investigation (DOI) is approximately

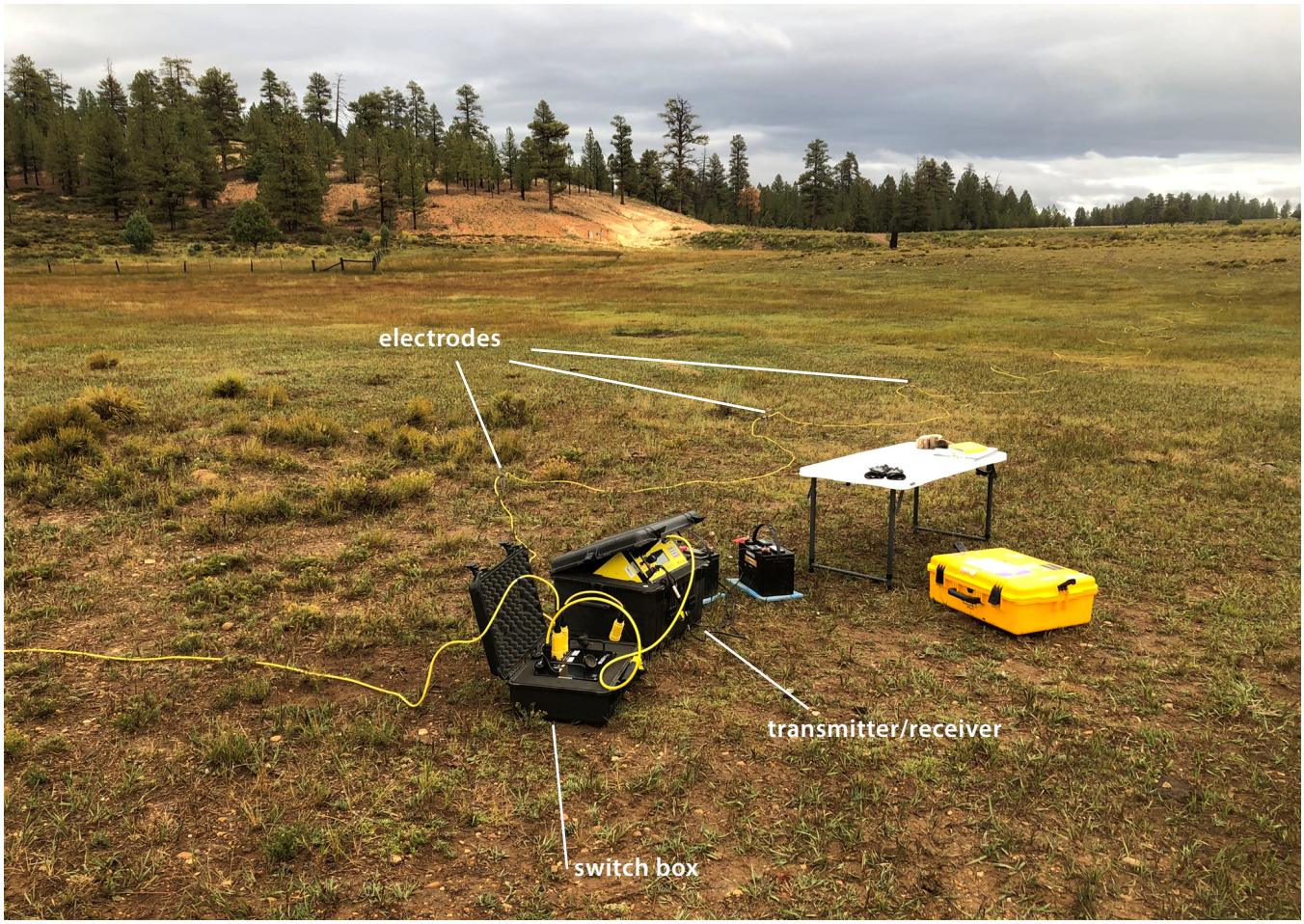

Figure 3. *Layout of ERT survey configuration for transect BRCA3; view to the east-southeast.*

25% of the total array length, but depends on the distribution of subsurface resistivities (Edwards, 1977). Actual DOI ranged from 17% to 24% of total array length. We measured contact resistance at each electrode and used saline water to reduce resistance to under 5000 ohm if necessary. We established location and elevation control at a subset of electrodes through post-processing of data collected with a Juniper Systems Geode GPS receiver and observed an average vertical accuracy of 50 cm. Relative elevation differences along each ERT transect were measured with a Leica DISTO™. ERT electrode location data are provided in Appendix A.

We processed and terrain-corrected the ERT survey results for elevation changes using EarthImager 2D software (AGI, 2020). This processing includes an inspection of raw data for quality assurance and an iterative process of 2D inversion modeling and noisy data filtering. We used a smooth model inversion which requires the smooth model complexity to be equal to or less than the true model complexity (Loke et al., 2003). During this iterative inversion modeling process, noisy data points are removed until the root mean square error (RMS) is below 10%. Each survey required five to eight iterations resulting in RMS below 5% and the retention of between 81% and 96% of data points. The normalized L2-norm parameter, another measurement of data misfit that indicates model convergence at values less than or equal to one, ranged from 0.9 to 1.73 (AGI, 2020). ERT data collection, processing, and modeling was conducted by the National Park Service; survey data quality and details on data processing for each survey are provided in Appendix B.

TEM Survey

TEM is a surface electromagnetic geophysical technique that has been used for groundwater exploration and investigations for decades (e.g., Fitterman and Stewart, 1986; Fitterman, 1989; Goldman et al., 1991; Fitterman et al., 1999; Christiansen et al., 2006; Fitterman and de Souza Filho, 2009; Hardwick et al., 2019). TEM is an active-source method that produces transient pulses of electric current and measures the attenuation signal of induced magnetic fields corresponding to changes in the electrical properties of subsurface materials. For a detailed description of the TEM method, refer to Kaufman and Keller (1983), McNeill (1990), and Fitterman and Labson (2005).

We conducted all TEM surveys with an ABEM WalkTEM ground loop system fitted with a 20 x 20-m transmitter antenna with high- and low-frequency receiver antenna coils capable of simultaneous recording (Figure 4). We surveyed three TEM transects centered on and orthogonal to the Rubys Inn fault composed of six unique stations each from June 1–2,

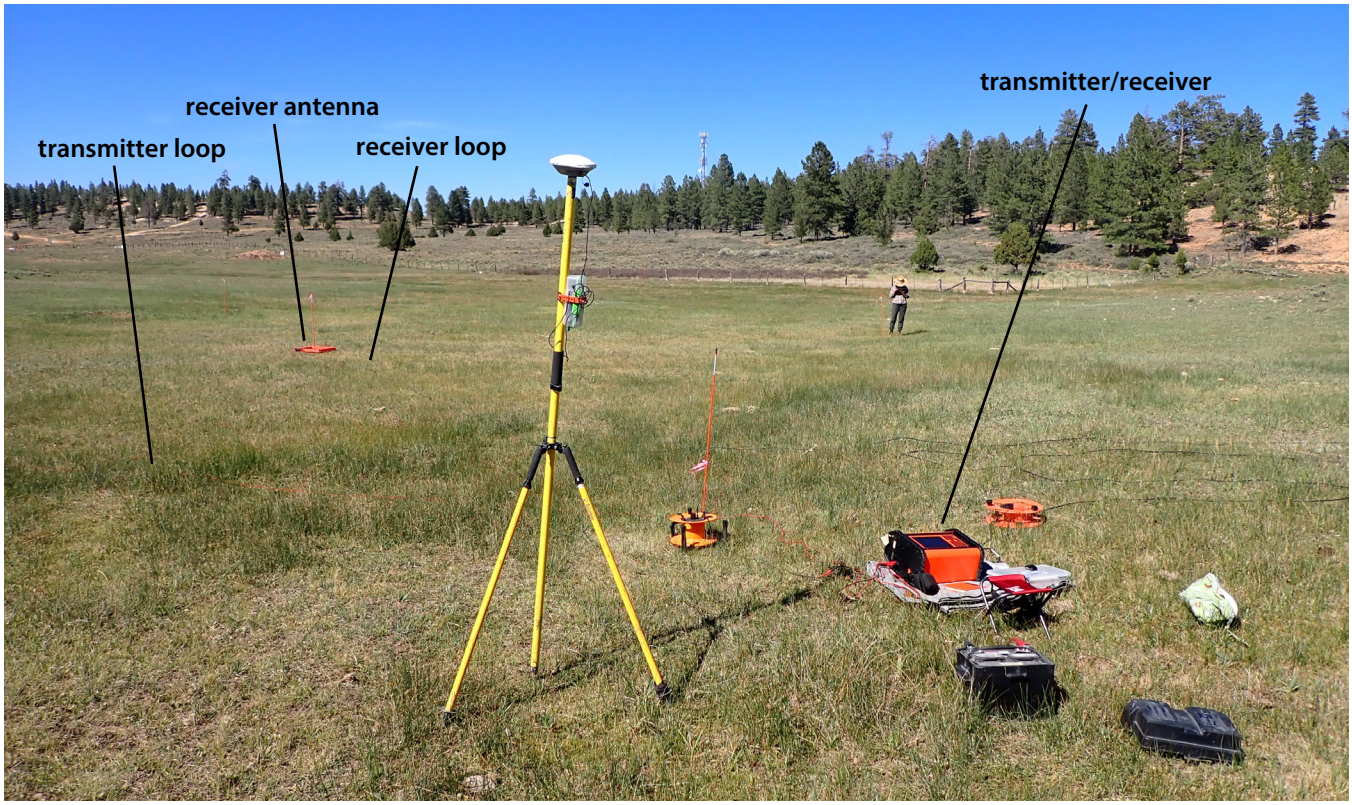

Figure 4. *Layout of TEM survey configuration for station BC09, view to the northeast. Transmitter loop and receiver loop are red and black cables in image, respectively.*

2022, and again from September 13–15, 2022 (Figure 1; Appendices C and D). We performed repeat soundings at each station using 150 ohm-m and 200 ohm-m in-line resistors to ensure adequate signal. We also performed repeat soundings at specific stations to ensure data consistency and quality for the duration of the field survey period. We established location and elevation control through post-processing of static data collected by Emlid Reach GNSS equipment and observed a vertical accuracy of better than 10 cm at all stations.

Of the June 2022 TEM surveys, eight stations produced very good quality soundings, eight stations produced sufficient soundings, and two stations produced poor soundings (Appendix C, Table C-2). Of the September 2022 TEM surveys, nine stations produced very good quality soundings, six stations produced sufficient soundings, and three stations produced poor soundings. Noise present in the sufficient- to poor-quality soundings is consistent with capacitive coupling, i.e., coherent noise from nearby man-made conductive features. Except for one station in June 2022 (BC11), soundings using the 150 ohm-m in-line resistor produced the best quality data. Sufficient- and poor-quality sounding data were processed to the extent feasible to utilize data from as many stations as possible in each transect.

After data processing, we created one-dimensional (1D) inversion models (Auken et al., 2015) (Appendix D) for every station and improved them until data fit was satisfactory, reaching a data residual of less than one standard deviation. Using 1D TEM inversion models, we created pseudo two-dimensional (2D) cross sections of resistivity to aid interpretations. The pseudo-2D cross sections display the 1D resistivity and are constrained using the DOI parameter (Spies, 1989; Christiansen and Auken, 2012). DOI is informed by the physical properties of subsurface materials and is therefore unique to each station.

RESULTS

Hydrogeologic Data

We acquired lithologic drilling logs for six monitoring wells in the study area; one of which (37W) is co-located with ERT and TEM measurements at the easternmost transect (BRCA1), four are within approximately 500 m (1650 ft) of BRCA1, and another (66W) roughly 2400 m west of the westernmost transect (Figure 1). The five wells clustered near the east and central transects are completed in sandstone, presumably the Straight Cliffs Formation. The wells range in depth from 44.2 to 59.4 m (145–195 ft). In these wells the alluvium-bedrock interface is found at depths of 9.1 to 21.3 m (30–70 ft) below ground surface (bgs) (Table 1). Depth to bedrock generally increases moving northward away from the fault zone as the alluvium thickens. At the well directly overlapping with geophysical measurements (37W), bedrock is encountered at 9.1 m (30 ft) bgs. The well along fault strike west of the geophysical measurements (66W) is 15.2 m (50 ft) deep and completed in alluvium.

Water-level measurements in the study area ranged from 3.5 to 7.3 m (11.6–24.1 ft) bgs in June 2022 and 3.8 to 7.5 m (12.3–24.5 ft) bgs in September 2022. Water levels in the study area generally decrease moving away from the Rubys Inn fault toward the center of Emery Valley; this interpretation is supported by Wallace et al. (2024) who created potentiometric surfaces for the entirety of Emery Valley. At the well directly overlapping with geophysical measurements (37W), groundwater is encountered at 3.5 to 3.8 m (11.6–12.3 ft) bgs. Historical records for these wells indicate that water levels have dropped by ~1.1 m since the 1980s (U.S. Geological Survey, 2023).

ERT Data

For ease of comparison across seasons, we rescaled resistivity model ranges for repeat transects to the scale of the survey with the lowest range of modeled resistivities. For the east transect, we rescaled survey lines BRCA1 and BRCA7 to the scale of BRCA1B (Figure 5). For the central transect, we rescaled survey line BRCA3B to the scale of BRCA3 (Figure 6).

East Transect

The resistivity models for BRCA1 and BRCA1B show the same structure and differ only in the maximum resistivities measured. The models indicate two main geologic layers were imaged northwest of the Rubys Inn fault zone (hanging wall) and five layers were imaged southeast of the fault zone (footwall) (Figure 5). A low-resistivity layer with values ranging from about 20 to 80 ohm-m exists at the surface northwest of the fault. This layer has resistivity values consistent with that of saturated, possibly clay-rich alluvium and extends to a depth of about 10 m bgs. At 10 m depth, the resistivity increases to about 120 to 600 ohm-m, consistent with sandstone and presumably the Straight Cliffs Formation. This change in resistivity at 10 m depth is also consistent with lithologic data that indicates bedrock at this depth in well 37W, which is located approximately 50 m from the northwest end of the transect (Figure 5). Water-level data from this well indicate that the water table is at 3.5 to 4.0 m depth; however, the shallow unsaturated zone is difficult to identify in the 10-m electrode spacing transects because this array is incapable of resolving features smaller than 5 m. This feature is more accurately resolved in the 4-m electrode spacing in transect BRCA7 (Figure 5C). Approaching the fault zone, both the shallow conductive layer and deeper resistive layer appear to dip more steeply to the southeast (Figure 5), consistent with mapping in the area (Biek et al., 2015). Additionally, surficial deposits at this point in the transect transition from Quaternary alluvium and colluvium (Qac) to a more resistive (100–600 ohm-m) presumably unsaturated Quaternary colluvium (Qc). Across the fault on the footwall, the data indicate five layers of differing resistivities, which we interpret as alternating layers of the white member and possibly underlying pink member of the Claron Formation. The uppermost and lowermost layers are highly resistive (200–9000 ohm-m in BRCA1 and 200–3000

ohm-m in BRCA1B) and likely limestone-dominant. Another possible lithology for the uppermost layer is the Tertiary conglomerate at Boat Mesa, which overlies the Claron and outcrops to the east-southeast of the study area. The remaining three layers are poorly to moderately resistive, ranging (from top to bottom) from 15–60 ohm-m to 60–200 ohm-m to 30–80 ohm-m. We interpret this as interbedded mudstone and siltstone within the Claron Formation. Without direct subsurface observations on this side of the fault, it is difficult to conclude whether the lower resistivity layers are saturated or unsaturated and clay rich. Also evident in the transect is the abrupt transition from steeply southeast-dipping layers to relatively flat layers within a short distance from the interpreted fault (~100 m), which is a well-documented feature of the Rubys Inn fault in this area (Lundin, 1989). The Rubys Inn fault zone itself appears to be ~80–100 m northwest of where the east

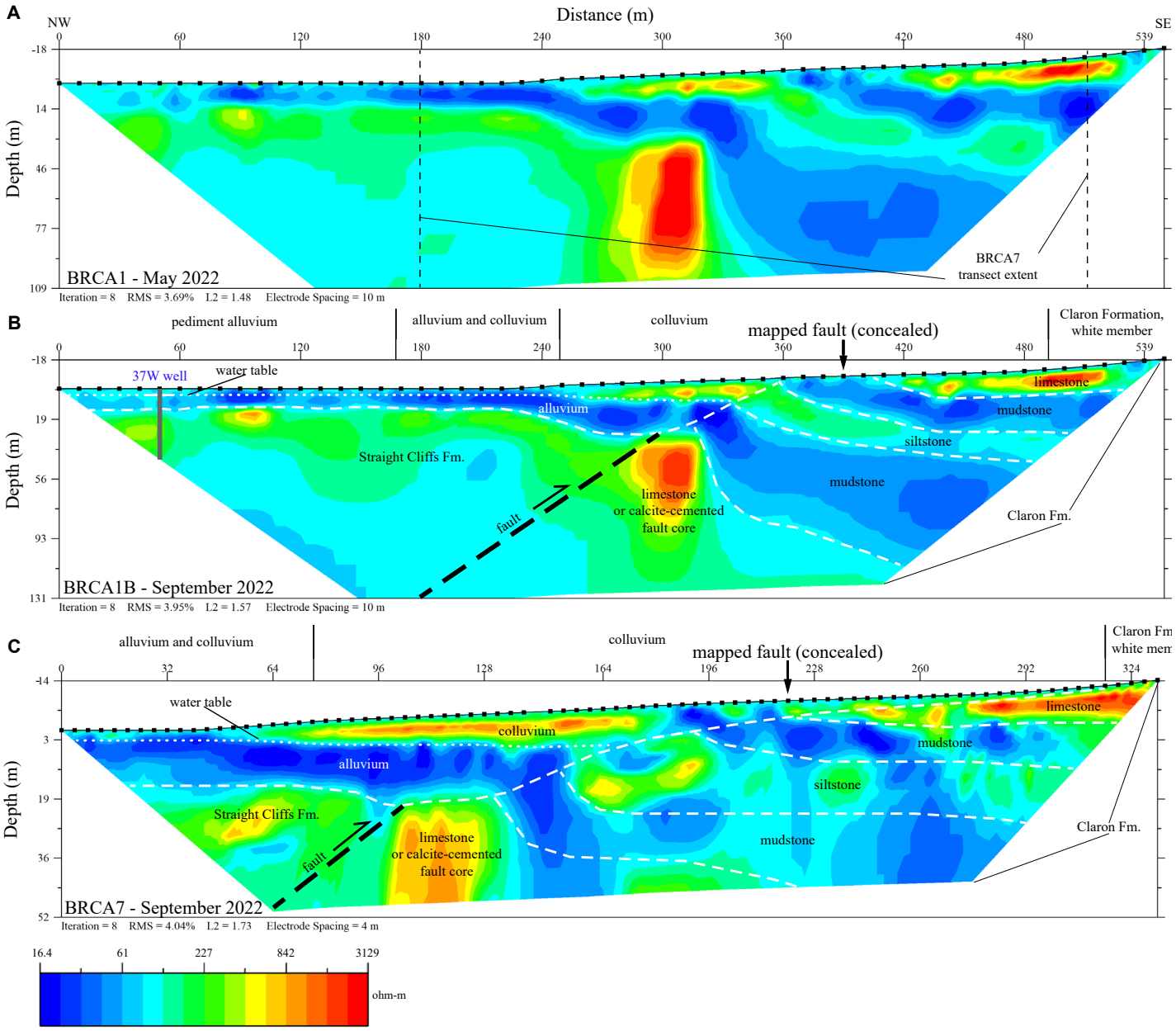

Figure 5. *Cross sections of the northwest- to southeast-trending electrical resistivity tomography (ERT) 10-m electrode spacing survey lines BRCA1 and BRCA1B and 4-m electrode spacing survey line BRCA7.* ***A)*** *2D inversion model results for survey line BRCA1 from May 2022.* ***B)*** *2D inversion model results for survey line BRCA1B from September 2022 with interpretation overlay.* ***C)*** *2D inversion model results for survey line BRCA7 from September 2022 with interpretation overlay. Surface geology as mapped by Biek et al. (2015) is labeled above cross sections B and C. Dashed white lines indicate lithologic contacts. Note that vertical scale differs between A, B, and C. Note that resistivity scale from BRCA1B applied to BRCA1 and BRCA7 for ease of comparison but maximum resistivity values for BRCA1 and BRCA7 are unrepresented.*

transect crosses the mapped fault. At ~35 m depth, this location has a zone of high-resistivity material ranging from 800 to 20,000 ohm-m. The high resistivity observed here could be evidence of a calcite-cemented fault core and damage zone, or of steeply dipping limestone bedding of the Claron Formation. Vertical to overturned bedding of the Claron Formation is documented to the northeast near the rim of Bryce Canyon National Park (Lundin, 1989).

Transect BRCA7 is centered on the mapped fault zone and the apparent fault zone as imaged by transect BRCA1. The reduced electrode spacing (4 m) and resulting higher resolution shows similar structures to the 10-m electrode spacing surveys but in greater detail (compare Figures 5A and 5B to 5C). At the surface of the northwest end of the transect, the data reveal a shallow (2–3 m) upper layer of moderate-resistivity (80–150 ohm-m) material above a low-resistivity zone; consistent with transects BRCA1 and BRCA1B, we interpret this as unsaturated alluvium overlying saturated alluvium.

Central Transect

Like BRCA1 and BRCA1B, the resistivity models for BRCA3 and BRCA3B generally differ mainly in maximum modeled resistivities. However, these models also exhibit seasonal hydrologic variation, discussed below. At the surface northwest of the mapped fault location is a ~4–5-m-thick layer of moderately high-resistivity (100–400 ohm-m) material that we interpret as unsaturated alluvium (Figure 6). Below this is a ~6–9-m-thick layer with lower resistivity (40–100 ohm-m) values consistent with saturated alluvium. At the bottom of this layer, at a depth of ~11–13 m, is a thick layer with resistivities of 170–400 ohm-m. This resistivity is consistent with sandstone of the Straight Cliffs Formation as interpreted in transects BRCA1 and BRCA1B. The surface at the southeast end of the transect is a moderate-resistivity layer (75–200 ohm-m) that we interpret as ~3 m of unsaturated alluvium. Below this layer are two highly contrasting offset layers that include a relatively high-resistivity layer (150–400 ohm-m)

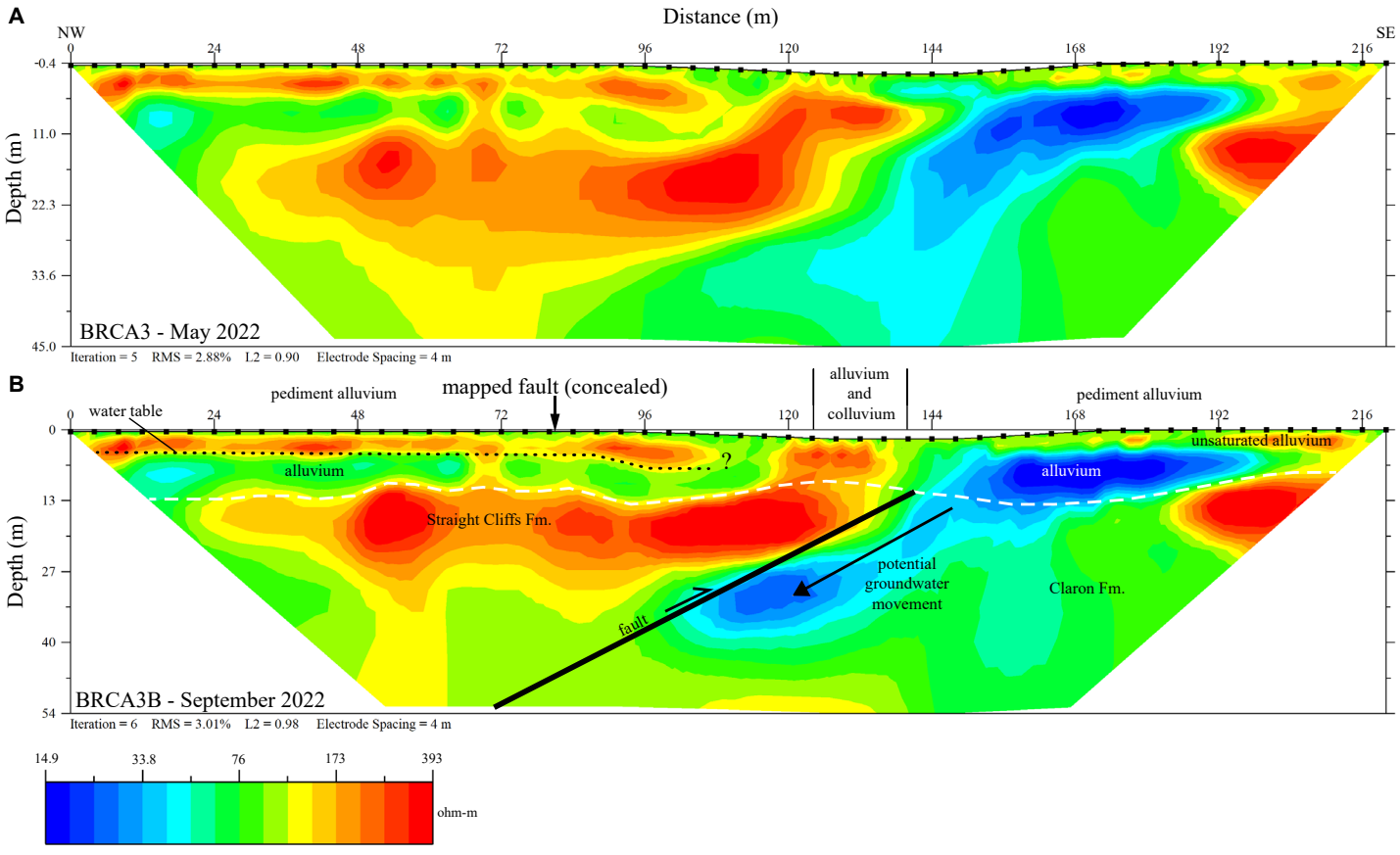

Figure 6. *Cross sections of the northwest- to southeast-trending electrical resistivity tomography (ERT) 4-m electrode spacing survey lines BRCA3 and BRCA3B.* ***A)*** *2D inversion model results for survey line BRCA3 from May 2022.* ***B)*** *2D inversion model results for survey line BRCA3B from September 2022 with interpretation overlay. Surface geology as mapped by Biek et al. (2015) is labeled above cross section. Dashed white line indicates lithologic contact. Note that vertical scale differs between A and B. Note that resistivity scale from BRCA3 applied to BRCA3B for ease of comparison but maximum resistivity values for BRCA3B are unrepresented.*

that is potentially limestone of the white member of the Claron Formation, and a low-resistivity layer (15–50 ohm-m) that is potentially saturated alluvium, saturated weathered limestone of the Claron Formation, or mudstone (saturated or unsaturated) of the Claron Formation. Without lithologic control on the footwall side of the fault, we are unsure of the thickness of the alluvium overlying the Claron Formation. A man-made pond is in a swale to the east-southeast of the transect; infiltration and lateral movement of water from this pond could be the source for saturation of the sediment and/or rock in the low-resistivity layer. The center-right of the transect has a northwest-dipping region of highly contrasting resistivities; we interpret this as the primary fault plane. The May 2022 resistivity model has a shallow low-resistivity zone coincident with a topographic low that is absent or diminished in the September resistivity model. In September, the low-resistivity layer that we identify as potentially saturated material appears to extend deeper into the subsurface along the fault plane. We suggest that this seasonal resistivity change shows downward groundwater movement through the footwall along the fault. Two other possibilities are that this groundwater movement is occurring on the hanging wall side of the fault, or through a damage zone along the fault plane. Although the fault is concealed at this location, the apparent fault location is ~70 m southeast of the mapped fault location. We see little evidence of bedrock dipping near the fault zone on either side, despite the transect being only ~300 m away from the east transect which exhibits evidence of dipping strata on both sides of the fault in resistivity models.

West Transect

The resistivity model for BRCA5 shows horizontal to sub-horizontal layering on each side of the fault zone (Figure 7). North of the fault zone in the hanging wall, we interpret an upper high-resistivity layer (200–10,000 ohm-m) as unsaturated colluvium and/or alluvium transitioning to Straight Cliffs Formation. Below this is a low-resistivity layer (5–30 ohm-m) that is likely Straight Cliffs Formation. The low resistivities could be attributed to groundwater saturation, clay-rich mudstone facies, or both. South of the fault zone in the footwall, we interpret interbedded limestone and mudstone of the pink member of the Claron Formation with alternating high (200–800 ohm-m; limestone) and low (5–50 ohm-m; mudstone) resistivities. There are no wells on the footwall side of the fault to constrain depth-to-water, so it is uncertain if the low-resistivity layers are saturated. The interbedded Claron layers are horizontal in the south of the transect but abruptly transition to steeply south-dipping (~45°) in the north-central region of the transect. We interpret these as drag folds that truncate at the primary fault plane. Biek et al. (2015) mapped Claron strata nearby dipping to the south as much as 80° in the footwall adjacent to the fault. They also mapped Straight Cliffs Formation strata of the hanging wall dipping to the south between 40° and 65°, which is not clearly discerned in the resistivity model. We interpret the resistivity model as showing the surface trace of the fault approximately 25 m north of the location mapped by Biek et al. (2015).

TEM Data

Like the ERT data, we scaled resistivity ranges for each TEM pseudo-2D cross section to be consistent across seasons. There is little difference in TEM resistivity measurements between seasons at each transect. Note that the resistivity scales differ between ERT and TEM due to the sensitivity of the different methods. We expect absolute resistivities to differ and overall relative contrasts to be similar. When comparing transects for both methods, "warm" colors indicate relative higher resistivity with both methods and "cool" colors indicate lower resistivity. The DOI for TEM stations are significantly limited due to the capacitive coupling identified in initial data processing.

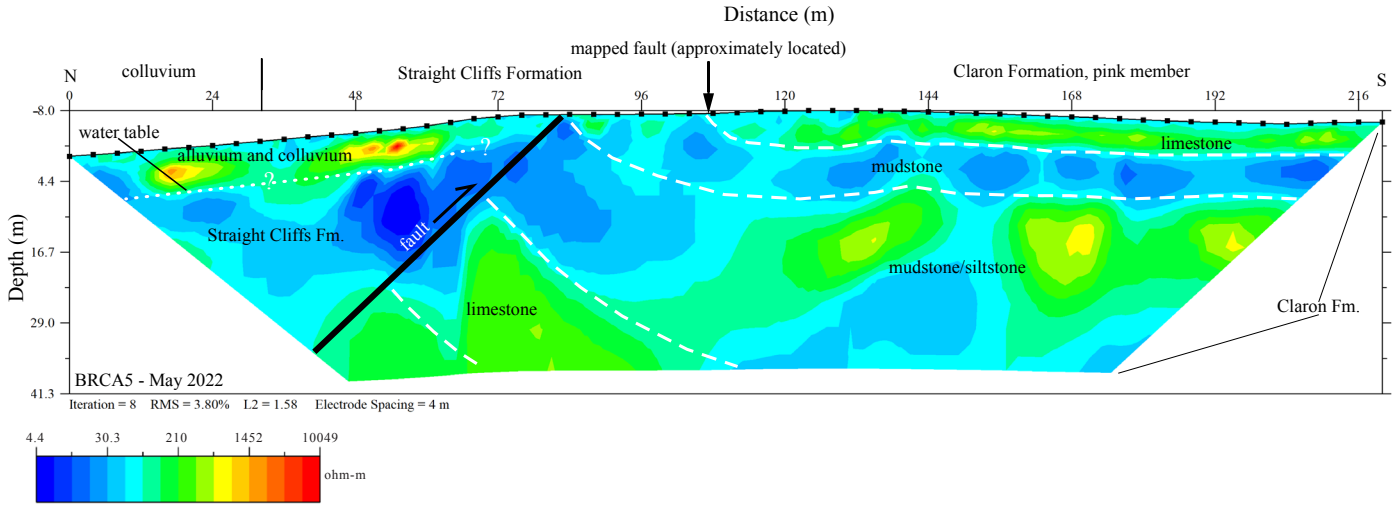

Figure 7. *Cross section of the north- to south-trending electrical resistivity tomography (ERT) 4-m electrode spacing survey line BRCA5. 2D inversion model results for survey line from May 2022 with interpretation overlay. Surface geology as mapped by Biek et al. (2015) is labeled above cross section. Dashed white lines indicate lithologic contacts.*

Capacitive coupling typically indicates the presence of something generating an electrical field which subsequently interferes with the electromagnetic readings (often man-made, likely buried in this case). As a result, we place lower confidence in the TEM models compared to the ERT models, especially in the central transect which yielded the most consistently problematic data (Appendix C). However, we were unable to identify any obvious causes of interference in the field area.

East Transect

Stations BC19 and BC18 at the northwest end of the transect indicate a shallow low-resistivity (<20 ohm-m) layer consistent with a saturated alluvium interpretation (Figure 8). This layer is ~3 m deep at station BC18, consistent with nearby water-level data, but at BC19 the lowest resistivity is at the surface, conflicting with data from co-located well 37W. Although TEM is capable of resolving meter-scale layers close to the surface, we do not have visual observations or hydrological data to corroborate the surface low-resistivity signal.

Stations BC19 and BC18, both in the hanging wall of the fault zone, indicate a higher resistivity layer (200–400 ohm-m) at ~9–10 m depth, consistent with lithologic well logs that indicate Straight Cliffs Formation at this depth. Below the interpreted Straight Cliffs Formation is a lower resistivity layer (40–80 ohm-m) that pinches out as it approaches the fault from a maximum thickness at BC19, although the thinning could be an artifact of the decreased DOI. This lower resistivity layer may reflect the fault plane itself, although this transect gives no other evidence of fault-related structures at any station. Across the interpreted fault, stations BC14, BC15, and BC16 indicate alternating layers of low (20 ohm-m) to moderate (80 ohm-m) and high (200–400 ohm-m) resistivity layers, which we interpret as interbedded mudstone, siltstone, and/or limestone layers in the white member and possibly the pink member of the Claron Formation.

Central Transect

All stations indicate a layer with low resistivity (10–30 ohm-m) consistent with the interpretation of saturated alluvium near the surface at ~2–3 m depth on both sides of the fault (Figure 9). Similarly, all stations reflect a transition to higher resistivity bedrock (100–300 ohm-m) at a depth of 8–10 m. This indication of bedrock is generally consistent with lithologic logs from the hanging wall. Stations BC12 and BC11 indicate a lower resistivity layer (30–60 ohm-m) at a depth of 45 m in the hanging wall. This lower resistivity layer trends upward approaching the fault zone and may reflect the fault plane. However, the central TEM transect yielded poor soundings across both seasons of data and we subsequently place low confidence in these models. The poor sounding quality at this transect may explain why the TEM failed to image the very low resistivity feature imaged with ERT along the same transect.

West Transect

Stations BC02 and BC03 (Figure 10), north of the fault zone, reflect a low resistivity layer from the surface to ~5 m depth, with the lowest resistivities (10 ohm-m) at ~2.5 m depth, possibly indicating the water table which pinches out approaching the fault. Historical water-level data from well 66W show that depth-to-groundwater was similar in the past to the depth inferred by TEM data (Table 1). Below this depth, these stations indicate a moderate resistivity layer (100 ohm-m) at ~10 m followed by a lower resistivity layer at ~25 m (30 ohm-m), which could be interpreted as sandstone and mudstone of the Straight Cliffs Formation, respectively.

Station BC04 shows a strong contrast in resistivity compared to stations BC02 and BC03 to the north (Figure 10). The southern four stations on this transect show an upper low-resistivity zone closer to the surface and a much higher-resistivity material directly beneath (100–200 ohm-m at 8–10 m depth) which we interpret as a limestone layer of the pink member of the Claron Formation. Stations BC05, BC06, and BC07 indicate moderate resistivity at the surface with very low resistivity at ~2 m depth (10 ohm-m). Without well constraint we cannot determine whether this reflects the water table and/or a clay-rich layer of the Claron Formation. The surface resistivity of the September survey is much lower than the June survey, which may be attributed to the precipitation during the time surrounding data collection. Resistivity decreases to moderate values (50–100 ohm-m) at ~40 m depth, which is likely a mudstone layer within the Claron. The strong contrast in resistivity and layer thickness between BC03 and BC04 implies a fault zone between these stations (i.e., thicker, more resistive material in the footwall). However, we are unable to resolve any structures within and around the fault.

DISCUSSION

Resistivity models for ERT transects produce clear depictions of the subsurface in both 10-m and 4-m electrode spacing layouts. The high resolution in these data makes features like alternating beds of differing resistivity or changes in the dip of stratigraphy readily apparent. For example, both 10-m and 4-m surveys of the east transect depict the transition from horizontal to gently dipping beds in an interpreted footwall drag fold. The higher data resolution and relatively clean data sets associated with these ERT surveys allow more-reliable interpretations of groundwater depth, stratigraphy, and structure within the study area relative to this study's TEM products.

Resistivity models from TEM soundings generally produce a deeper DOI than ERT data and are better able to detect slightly deeper features. However, the scale of features associated with the Rubys Inn fault appears to be too small for clear detection with the spacing of TEM soundings selected for our transects. For example, the complicated structural signals associated with the fault zone in the eastern transect (Figure 5) change too rapidly over a short distance and are completely overwhelmed by the stronger lateral signals of the dominant lithologies (Figure 8).

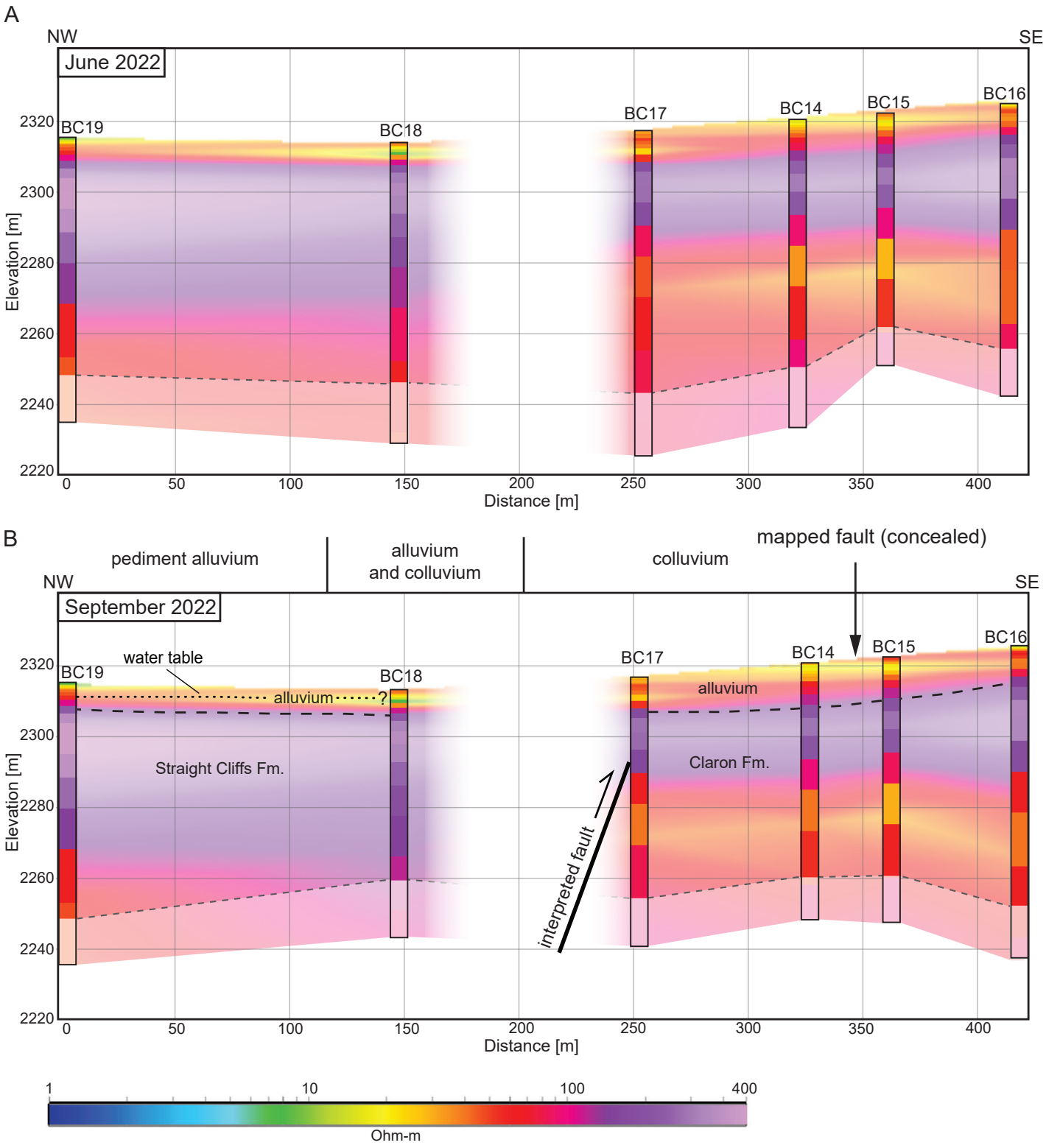

Figure 8. *Cross sections of northwest- to southeast-trending transient electromagnetic (TEM) data for the eastern transect. TEM stations and 1D inversion models are indicated with solid colors and outlines; faded colors indicate interpolation between soundings. Well 37W is co-located with station BC19. Gray dashed line indicates conservative depth of investigation.* ***A)*** *Inversion model pseudo-2D transect results from June 2022.* ***B)*** *Inversion model pseudo-2D transect results from September 2022 with interpretation overlay. Surface geology as mapped by Biek et al. (2015) is labeled above the cross section.*

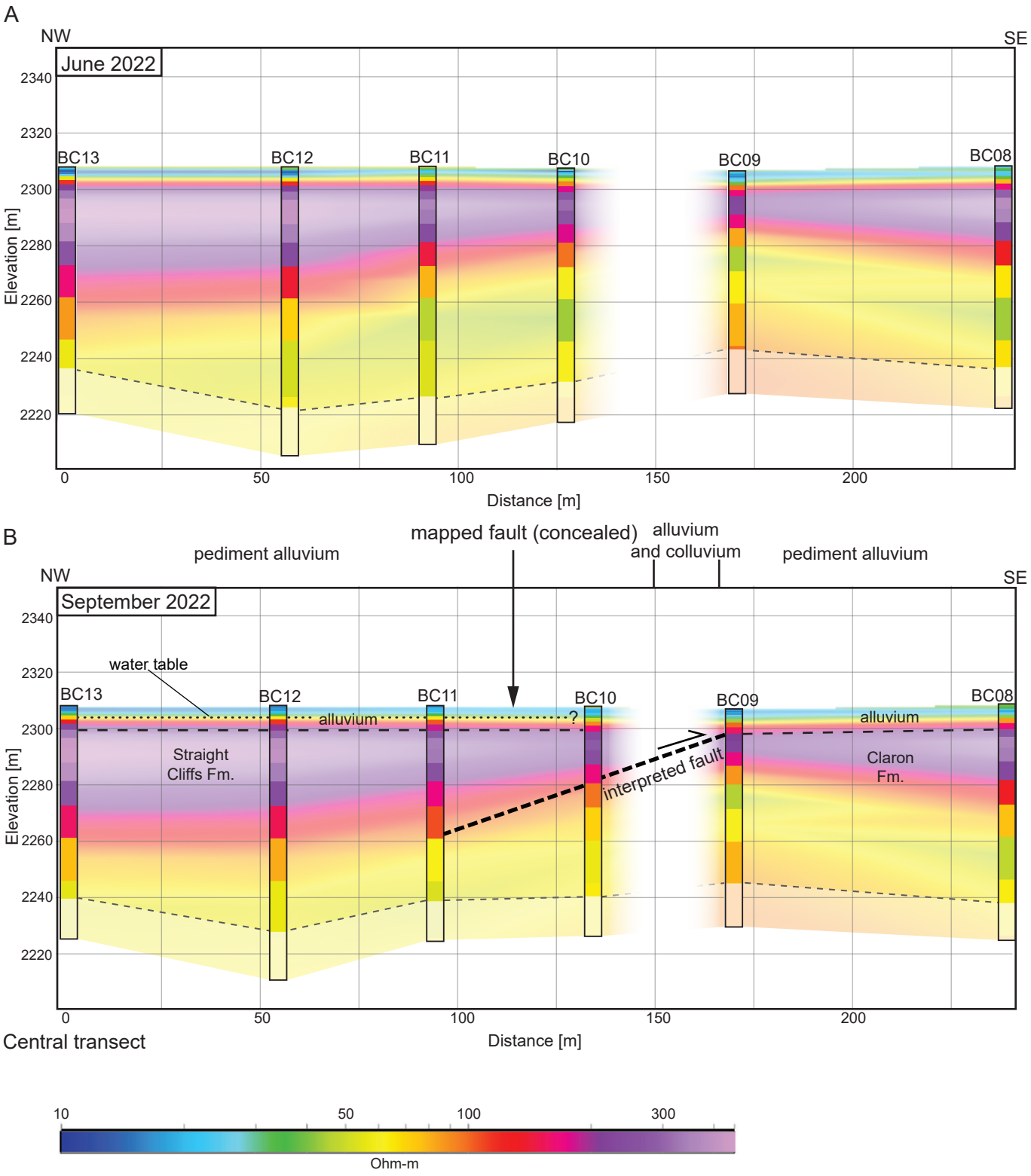

Figure 9. *Cross sections of northwest- to southeast-trending transient electromagnetic (TEM) data for the central transect. TEM stations and 1D inversion models are indicated with solid colors and outlines; faded colors indicate interpolation between soundings. Gray dashed line indicates conservative DOI.* ***A)*** *Inversion model pseudo-2D transect results from June 2022.* ***B)*** *Inversion model pseudo-2D transect results from September 2022 with interpretation overlay. Surface geology as mapped by Biek et al. (2015) is labeled above the cross section.*

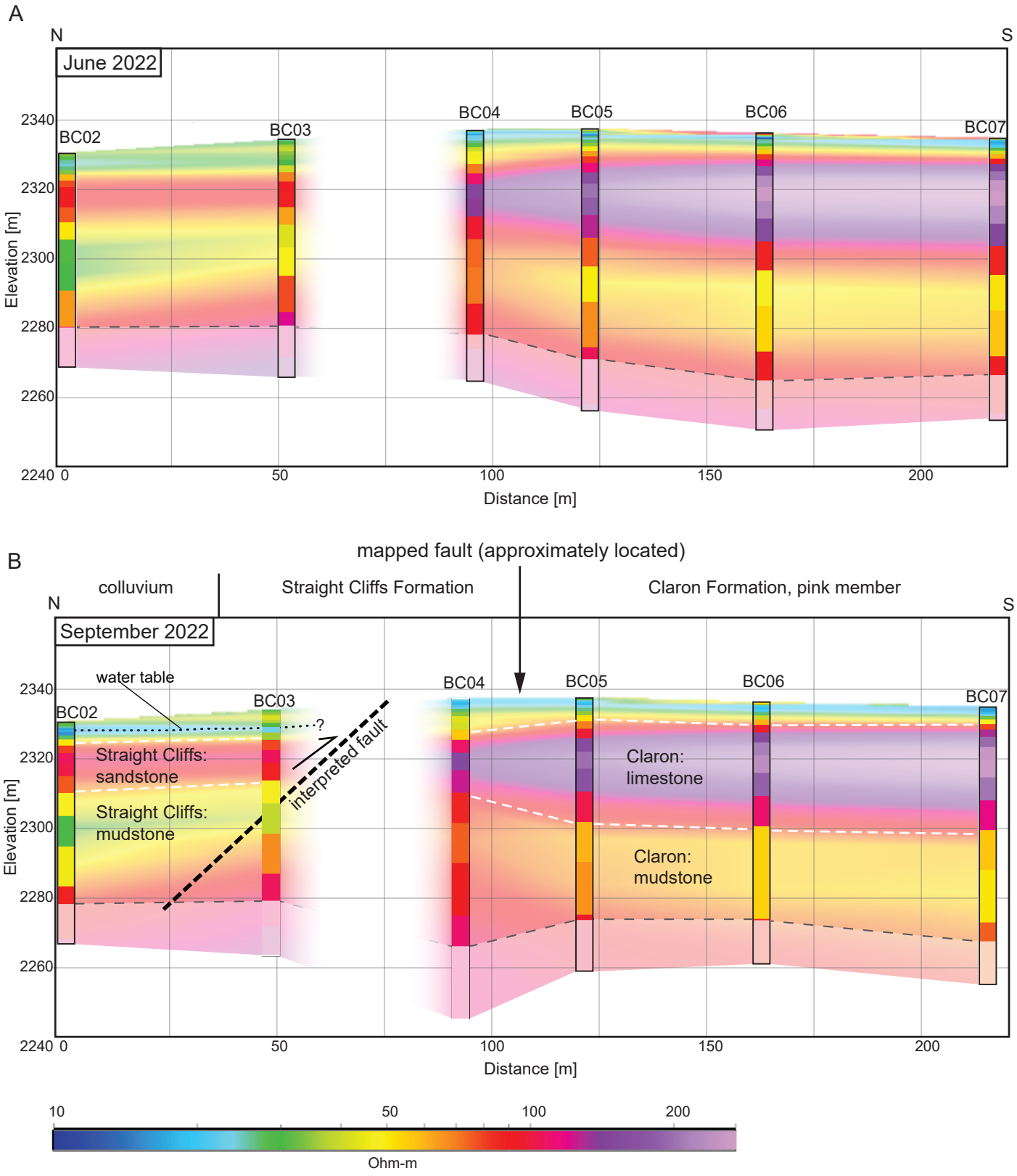

Figure 10. *Cross sections of north- to south-trending transient electromagnetic (TEM) data for the western transect. TEM stations and 1D inversion models are indicated with solid colors and outlines; faded colors indicate interpolation between soundings. Gray dashed line indicates conservative DOI.* ***A)*** *Inversion model pseudo-2D transect results from June 2022.* ***B)*** *Inversion model pseudo-2D transect results from September 2022 with interpretation overlay. Surface geology as mapped by Biek et al. (2015) is labeled above the cross section.*

In instances where TEM fails to image strong lateral signals, e.g., the low-resistivity portion of the central transect (Figures 6 and 9), we attribute this to the capacitive coupling interference present in over half of the TEM soundings. TEM is substantially more sensitive to electromagnetic interference or unseen conductors compared to ERT and the clear presence of this interference results in TEM models which are less reliable for interpreting the shallow stratigraphy and structure of the study area. In general, we found the TEM data to be a useful secondary tool for corroborating and interpreting the ERT data, but difficult to interpret in isolation.

The Rubys Inn fault is concealed at the surface over a significant portion of our study area. Our data constrain the actual fault location to as much as 70–100 m off from the mapped location perpendicular to strike. This difference is likely due to the inherent uncertainty associated with the original map scale (1:62,500). These transects can be used to accurately site and appropriately design monitoring wells near the fault which would enable an improved understanding of this fault's hydrogeologic control through aquifer testing, groundwater sampling, and groundwater level monitoring. Our findings also raise the possibility that our transects are not truly perpendicular to strike, which would have implications on our interpretations of bedrock and fault dip.

East Transect

Although the TEM inversion models identify both the groundwater level and alluvium-bedrock contact in the hanging wall to a sufficient degree, the ERT inversion models yield more-refined contacts and geometries, especially BRCA7 (4-m electrode spacing, Figure 5C). Although the land surface gradient and potentiometric surface gradient of Wallace et al. (2024) are to the northwest, the contact between what we identify as saturated alluvium and Straight Cliffs Formation dips to the southeast near and northwest of what we interpret as the primary fault plane. The low-resistivity layer (20–80 ohm-m) continues horizontally across the fault zone before dipping steeply to the southeast again. Across the fault zone in the footwall, we interpret this low-resistivity layer as a steeply dipping drag fold of clay-rich mudstone or siltstone facies of the Claron Formation, but it is plausible that the low resistivity could also be attributed to flow from what we know is saturated alluvium above the hanging wall. Without well data closer to the fault zone or in the footwall, the location of groundwater and hydraulic gradient are uncertain.

Central Transect

Both the ERT and TEM inversion models adequately depict the groundwater level and depth to bedrock in the hanging wall based on water-level and lithologic constraints from nearby wells. Conversely, without observed data in the footwall, we are uncertain of the lithology of the near-surface low-resistivity layer (15–50 ohm-m) (Figure 6). Given the proximity to the Quaternary fluvial channel (Qac on Figure 1) and pond to the southeast, our preferred interpretation is that the low-resistivity zone consists of saturated alluvium, although the depth of the underlying sediment-bedrock interface is unclear. Additionally, given the seasonal variation in location and extent of the low-resistivity layer that trends downward along the interpreted fault plane, the ERT inversion models suggest that groundwater may be flowing to the northwest down-dip along the fault. However, another possible interpretation is that the low resistivity along the interpreted fault plane represents clay-rich fault gouge in the damage zone of the footwall, discussed below (Figures 11 and 12).

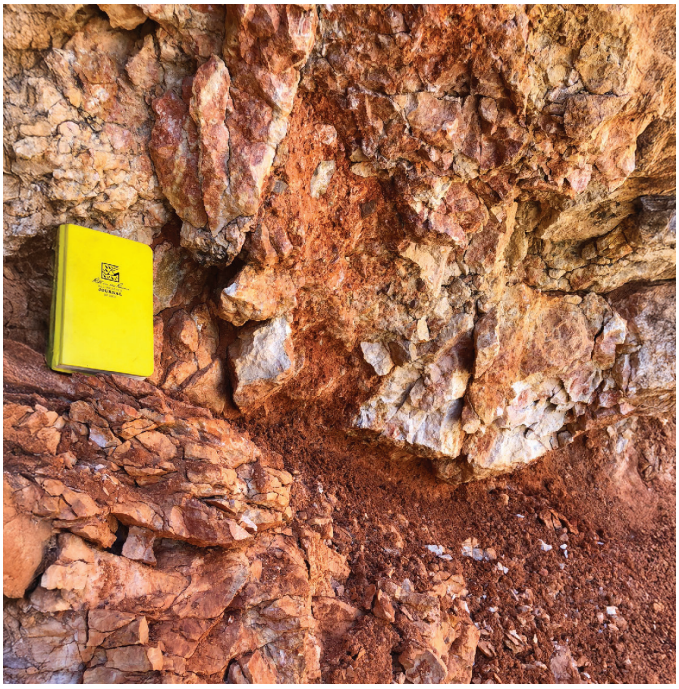

Figure 11. *Close-up view of Claron-over-Claron fault exposure at east end of Rubys Inn thrust; location shown in Figure 1. The fault plane is the dark rust-colored diagonal band. Note fault gouge and extensive brecciation in both hanging wall and footwall.*

Figure 12. *View to the west of east end of Rubys Inn thrust; location shown in Figure 1. Fault gouge and brecciation are extensive in the footwall but the visible hanging wall fault plane is well-indurated and striated.*

Determining the lithology and hydrogeologic control of low-resistivity material in the fault zone requires further study (e.g., direct observation of subsurface materials from drilling and/or aquifer testing).

West Transect

Without adequate water-level constraint near the west transect, neither ERT nor TEM inversion models confidently locate groundwater depth on either side of the thrust fault at the west transect. Both ERT and TEM inversion models identifies high-, moderately high-, and low-resistivity layers on both sides of the fault; the highest contrast occurs in the hanging wall, at what is either a sediment/bedrock interface, interface between facies of the Straight Cliffs Formation, or the water table. Unlike the previously discussed transects, the lower contrast between resistivities along the apparent fault plane makes interpretation more difficult. One possibility is that the lowest resistivity zone (<10 ohm-m) shown in the hanging wall (Figure 7) is indicative of clay-rich fault gouge. In this case, we would assume reduced permeability and a reduction of across-fault groundwater flow in this region. However, without hydrogeologic control, we cannot reduce uncertainty in this interpretation.

Evidence of Deformation

Inversion models for our ERT surveys produce clear depictions of the subsurface for all transects. The high resolution in these data makes features like alternating beds of differing lithology and resistivity, changes in the dip of stratigraphy, or changes in groundwater occurrence readily apparent. For example, both 10-m and 4-m surveys of the east transect depict the transition from horizontal to gently dipping beds in the interpreted footwall drag fold. Deformation in the footwall of the Rubys Inn fault is well documented in Hillsdale Canyon, approximately 15 km to the west of the study area. Cleveland et al. (2014) observed deformation bands, cataclastic flexural slip, and plastically deformed petrified wood in the flexural slip zone all within the Wahweap Formation. These features and processes often reduce permeability in similar lithologies (Bense et al., 2013). Although there are no sufficient outcrops to observe whether these same processes are apparent in the Straight Cliffs Formation in our study area, the two formations have a similar lithology and formed in a similar depositional environment. Deformation in the fault zone is also well documented at the eastern end of the fault, along Utah Highway 12 in the Tropic Amphitheater (Figure 1). Here, Lundin (1989) observed minor thrust faults, conjugate fracture sets, and fault breccia in the hanging wall and footwall, both consisting of the pink member of the Claron Formation. He also observed a 10-cm-thick fault gouge zone. We observed this zone of fault gouge, as well as extensive fault breccia and fractures extending into both the hanging wall and footwall (Figures 11 and 12). Though fracturing and brecciation can enhance fault zone permeability parallel to the fault plane, cataclastic brecciation and fault gouge can reduce permeability perpendicular to the fault plane (Bense et al., 2013). It is important to note that the scale of these features may be below the resolution of our ERT surveys. Future drilling and geologic sampling can make up for such resolution limitations. Drilling observations will then help reduce uncertainty in ERT-based interpretations away from drilling sites.

SUMMARY

Groundwater resources in the Paunsaugunt Plateau and Emery Valley, Garfield County, Utah, support domestic, municipal, and ecological uses in Bryce Canyon National Park and adjacent communities, including Bryce Canyon City. Emery Valley is experiencing increased water demand from tourism-related development. Such development exacerbates possible climate-related threats to groundwater resources and groundwater-dependent ecosystems in and around Bryce Canyon National Park. The goal of this study was to improve the understanding of the hydrogeologic role of the Rubys Inn fault and whether this fault affects groundwater flow to nearby springs and seeps and compartmentalizes groundwater in BCNP from nearby groundwater pumping in Emery Valley.

To identify the presence of groundwater, detect groundwater level changes, and characterize the fault zone, we conducted three ERT surveys and three TEM surveys each during spring (May/June) and fall (September) 2022. We produced 2D ERT inversion models and pseudo-2D transects using 1D TEM inversion models for each survey line. The Rubys Inn fault is concealed at the surface over a significant portion of our study area. The results of our geophysical surveys show that the mapped fault location is as much as 70–100 m off from the actual location perpendicular to strike.

Lithologic logs and water-level data from nearby wells support our interpretations of groundwater levels and stratigraphy on the hanging wall side of the fault. Resistivity models identify saturated and unsaturated alluvium and colluvium overlying Straight Cliffs Formation sandstone and mudstone in the hanging wall and Claron Formation limestone, mudstone, and siltstone in the footwall. Structural features like the primary fault plane and a footwall drag fold are also interpreted in the inversion models.

ERT results suggest minor hydrologic differences can be attributed to seasonality of precipitation and groundwater recharge. Depth to groundwater is well constrained by well data in the hanging wall of the east and central transects. Though we identify conductive layers near the surface of the footwall in each transect, without nearby well data, we are uncertain if these represent groundwater and/or differences in lithology.

Geophysical data illustrate the complexity and variability of the Rubys Inn fault within a relatively short distance along strike.

Based on the variable contrasts in resistivities and likely lithologic properties observed in this study, as well as diverse observations from previous Rubys Inn fault studies, we infer that the fault likely has variable barrier/conduit characteristics with respect to groundwater flow. Further investigation into the hydrogeologic role of the Rubys Inn fault is needed to verify this interpretation, including collecting geologic samples via drilling one or more boreholes through the fault plane and/or into the footwall, as well as installing monitoring wells to conduct aquifer tests, collect groundwater samples, and monitor groundwater levels adjacent to the fault zone. Our results will be critical for accurately siting and appropriately designing such wells.

ACKNOWLEDGMENTS

This work is funded by the National Park Service (NPS) and the Utah Geological Survey (UGS) as part of grant #P22AC00931-00. We thank Christian Hardwick, Will Hurlbut, and Skadi Kobe (UGS) and Tyler Gilkerson, Nicole O'Shea, Jeffrey Hughes, Steve Rice, and Tyra Olstad (NPS) for valuable assistance with geophysical data collection, processing, and study design. Tyler Knudsen (UGS) contributed insightful field observations of the study area. We thank Ruby's Inn for access to their land and monitoring wells. Lucy Jordan (UGS) and Rhiannon Garrard (NPS) provided a helpful review of this document.

REFERENCES

Advanced Geosciences Incorporated, 2020, AGI EarthImager 2D: https://www.agiusa.com/agi-earthimager-2d, accessed October 2022.

Archie, G.E., 1942, The electric resistivity log as an aid in determining some reservoir characteristics: Transactions AIME, v. 146, no. 1, p. 54–62.

Auken, E., Christiansen, A.V., Kirkegaard, C., Fiandaca, G., Schamper, C., Behroozmad, A.A., Binley, A., Nielsen, E., Efferso, F., Christensen, N.B., Sorensen, K., Foged, N., and Vignoli, G., 2015, An overview of a highly versatile forward and stable inverse algorithm for airborne, ground-based and borehole electromagnetic and electric data: Exploration Geophysics, v. 46, p. 223–235.

Ball, L.B., Ge, S.M., Caine, J.S., Revil, A., and Jardani, A., 2010, Constraining fault-zone hydrogeology through integrated hydrological and geoelectrical analysis: Hydrogeology Journal, v. 18, p. 1057–1067.

Barnes, H., Hinojosa, J.R., Spinelli, G.A., Mozley, P.S., Koning, D., Sproule, T.G., and Wilson, J.L., 2021, Detecting fault zone characteristics and paleovalley incision using electrical resistivity—Loma Blanca Fault, New Mexico: Geophysics, v. 86, p. 1MJ–WA152.

Bense, V. F., Gleeson, T., Loveless, S.E., Bour, O., and Scibek, J., 2013, Fault zone hydrogeology: Earth-Science Reviews, v. 127, p. 171–192.

Biek, B., Rowley, P.D., Anderson, J.J., Maldanado, F., Moore, D.W., Hacker, D.B., Eaton, J.G., Hereford, R., Sable, E.G., Filkhorn, H.F., and Matyjasik, B., 2015, Geologic map of the Panguitch 30′ x 60′ quadrangle, Garfield, Iron, and Kane Counties, Utah: Utah Geological Survey Map M-270dm, 1:62,500 scale, https://doi.org/10.34191/M-270DM.

Binley, A., and Slater, L., 2020, Resistivity and induced polarization—theory and applications to the near-surface Earth: Cambridge, Cambridge University Press, 408 p.

Bowers, W.E., 1990, Geologic map of Bryce Canyon National Park and vicinity, southwestern Utah: U.S. Geological Survey Miscellaneous Investigations Series Map I-2108, 15 p., 1 plate, scale 1:24,000.

Caine, J.S., Evans, J., and Forster, C.B., 1996, Fault zone architecture and permeability structure: Geology, v. 24, p. 1025–1028.

Caputo, R., L. Salviulo, S.P., and Loperte, A., 2007, Late Quaternary activity along the Scorciabuoi Fault (southern Italy) as inferred from electrical resistivity tomographies: Annals of Geophysics, v. 50, p. 213–224.

Christiansen A.V., Auken E., Sørensen K., 2006, The transient electromagnetic method, *in* Kirsch R., editor, Groundwater Geophysics: Berlin, Springer, https://doi.org/10.1007/3-540-29387-6_6.

Christiansen, A.V., and Auken, E., 2012, A global measure for depth of investigation: Geophysics, v. 77, no. 4, p. WB171–WB177.

Cleveland, C., Garrard, R.M., McLemore, D.M., Yon, J.C.E., Kidman, G., and MacLean, J.S., 2014, Strain accommodation in the footwall of the Rubys Inn thrust fault, Hillsdale Canyon, southern Utah: The Compass—Earth Science Journal of Sigma Gamma Epsilon, v. 86, p. 102–117.

Davis, G.H., and Krantz, R.W., 1986, Post-Laramide thrust faults in the Claron Formation, Bryce Canyon National Park, Utah [abs.]: Geological Society of America Abstracts with Programs, v. 18, p. 98.

Davis, G.H., 1999, Structural geology of the Colorado Plateau region of southern Utah, with special emphasis on deformation bands: Geological Society of America Special Paper 342, 157 p.

Edwards, L.S. 1977, A modified pseudosection for resistivity and IP: Geophysics, v. 42, p. 1020–1036.

Fitterman, D.V., 1989, Detectability levels for central induction transient soundings: Geophysics, v. 54, p. 127–129.

Fitterman, D.V., Deszcz-Pan, M., and Stoddard, C.E., 1999, Results of time-domain electromagnetic soundings in Everglades National Park, Florida (on CD–ROM): U.S. Geological Survey Open-File Report 99–426, 152 p.

Fitterman, D.V., and Labson, V.F., 2005, Electromagnetic induction methods for environmental problems, *in* Butler, D.K., editor, Near surface geophysics, part 1—Concepts and fundamentals: Tulsa, Oklahoma, Society of Exploration Geophysicists, p. 295–349.

Fitterman, D.V., and de Souza Filho, O.A., 2009, Transient electromagnetic soundings near Great Sand Dunes National Park and Preserve, San Luis Valley (2006 Field Season), Colorado: U.S. Geological Survey Open-File Report 2009-1051, https://doi.org/10.3133/ofr20091051.

Fitterman, D.V., and Stewart, M.T., 1986, Transient electromagnetic sounding for ground-water: Geophysics, v. 51, p. 995–1005.

Goldman, M., Gilad, D., Ronen, A., and Melloul, A., 1991, Mapping seawater intrusion into the coastal aquifer of Israel by the time domain electromagnetic method: Geoexploration, v. 28, p. 153–174.

Hardwick, C., Hurlbut, W., and Gwynn, M., 2019, Geophysical surveys of the Milford, Utah, FORGE site—gravity and TEM, *in* Allis, R., and Moore, J.N., editors, Geothermal characteristics of the Roosevelt Hot Springs system and adjacent FORGE EGS site, Milford, Utah: Utah Geological Survey Miscellaneous Publication 169-F, 14 p., https://doi.org/10.34191/MP-169-F.

Johnson, T.C., Versteeg, R.J., Ward, A., Day-Lewis, F.D., and Revil, A., 2010, Improved hydrogeophysical characterization and monitoring through parallel modeling and inversion of time-domain resistivity and induced polarization data: Geophysics, v. 75, p. 1JA–Z98.

Kaufman, A.A., and Keller, G.V., 1983, Frequency and transient sounding: Amsterdam, Elsevier, 685 p.

Lawton, T.F., Pollock, S.L., and Robinson, R.A.J., 2003, Integrating sandstone petrology and nonmarine sequence stratigraphy—application to the Late Cretaceous fluvial systems of southwestern Utah, U.S.A.: Journal of Sedimentary Research, v. 73, no. 3, p. 389–406.

Leavitt, R.E., May, S.B., and MacLean, J.S., 2011, Preliminary field investigation into the relationship between hoodoo formation and footwall shearing of the Ruby's Inn thrust fault, Bryce Canyon, Utah [abs.]: Geological Society of America Abstracts with Programs, v. 43, no. 5, p. 296.

Loke, M.H., Acworth, I., and Dahlin, T., 2003, A comparison of smooth and blocky inversion methods in 2D electrical imaging surveys: Exploration Geophysics, v. 34, p. 182–187.

Lundin, E.R., 1989, Thrusting of the Claron Formation, the Bryce Canyon region, Utah: Geological Society of America Bulletin, v. 101, p. 1038–1050.

May, S.B., Leavitt, R.E., and MacLean, J.S., 2011, Extent of footwall shear adjacent to the Ruby's Inn thrust fault, southern Utah [abs.]: Geological Society of America Abstracts with Programs, v. 43, no. 5, p. 116.

McNeill, J.D., 1990, Use of electromagnetic methods for groundwater studies, *in* Ward, S.H., editor, Geotechnical and environmental geophysics: Tulsa, Oklahoma, Society of Exploration Geophysicists, p. 191–218.

Merle, O.R., Davis, G.H., Nickelsen, R.P., and Gourlay, P.A., 1993, Relation of thin-skinned thrusting of Colorado Plateau strata in southwestern Utah to Cenozoic magmatism: Geological Society of America Bulletin, v. 105, p. 387–398.

Nabighian, M.N., and Macnae, J.C., 1991, Time domain electromagnetic prospecting methods, Chapter 6, *in* Nabighian, M.N., editor, Electromagnetic methods in applied geophysics, Volume 2—Applications part A: Tulsa, Oklahoma, Society of Exploration Geophysicists, Investigations in Geophysics Series, p. 427–520.

Nickelsen, R.P., and Merle, O., 1991, Structural evolution at the tip line of a mid-Tertiary compressional event in southwestern Utah [abs.]: Geological Society of America Abstracts with Programs, v. 23, no. 1, p. 109.

Nickelsen, R.P., Merle, O., and Davis, G.H., 1992, Structures of the mid-Tertiary radial compression in the High Plateaus of southern Utah in relation to Sevier, Laramide, and Basin and Range deformation [abs.]: Geological Society of America Abstracts with Programs, v. 24, no. 6, p. 55.

Palacky, G.J., 1988, Resistivity characteristics of geologic targets, Chapter 3, *in* Nabighian, M.N., editor, Electromagnetic methods in applied geophysics—Volume 1, Theory: Tulsa, Okla., Society of Exploration Geophysicists, Investigations in Geophysics Series, p. 52–129.

Saribudak, M., and Hawkins, A., 2019, Hydrogeophysical characterization of the Haby Crossing Fault, San Antonio, Texas, USA: Journal of Applied Geophysics, v. 162, p. 164–173.

Singha, K., Day-Lewis, F.D., Johnson, T., and Slater, L.D., 2014, Advances in interpretation of subsurface processes with time-lapse electrical imaging: Hydrological Processes, v. 29, 28 p.

Spies, B., 1989, Depth of investigation in electromagnetic sounding methods: Geophysics, v. 54, no. 7, p. 872–888.

Suzuki, K., Toda, S., Kusunoki, K., Fujimitsu, Y., Mogi, T., and Jomori, A., 2000, Case studies of electrical and electromagnetic methods applied to mapping active faults beneath the thick Quaternary: Engineering Geology, v. 56, p. 29–45.

U.S. Geological Survey, 2023, USGS water data for the Nation: U.S. Geological Survey National Water Information System database, https://doi.org/10.5066/F7P55KJN, accessed August 2023.

Utah Division of Water Rights, 2022, Well-drilling database: https://waterrights.utah.gov/wellInfo/wellInfo.asp, accessed July 2022.

Wallace, J., and Schlossnagle, T.H., 2021, Petition for groundwater quality classification, Bryce Canyon area, Garfield County, Utah: Utah Department of Environmental Quality, Division of Water Quality Aquifer Classification Petition Document, 46 p.

Wallace, J., Schlossnagle, T.H., Ladig, K., Inkenbrandt, P.C., Hurlow, H.A., and Hardwick, C., 2024, Characterization of groundwater in Johns and Emery Valleys, Garfield and Kane County, Utah, with emphasis on the groundwater budget and groundwater-surface water interaction: Utah Geological Survey Special Study 172, 106 p., https://doi.org/10.34191/SS-172.

Wise, D.J., Cassidy, J., and Locke, C.A., 2003, Geophysical imaging of the Quaternary Wairoa North Fault, New Zealand—A case study: Journal of Applied Geophysics, v. 53, p. 1–16

Zohdy, A.A.R., Eaton, G.P., and Mabey, D.R., 1974, Application of surface geophysics to ground-water investigations: U.S. Geological Survey Techniques of Water-Resources Investigations, Book 2, Chapter D1, 116 p.

APPENDICES

APPENDIX A

Electrical Resistivity Tomography Location Data

Link to supplemental data download:

https://ugspub.nr.utah.gov /publications/reports_of_investigations/ri-290/ri-290a.xlsx

APPENDIX B

Electrical Resistivity Tomography Model Inversions and Data Residuals

Link to supplemental data download:

https://ugspub.nr.utah.gov/publications/reports_of_investigations/ri-290/ri-290b.pdf

APPENDIX C

Transient Electromagnetic Location Data and Data Quality

Link to supplemental data download:

https://ugspub.nr.utah.gov/publications/reports_of_investigations/ri-290/ri-290c.xlsx

APPENDIX D

Transient Electromagnetic Model Inversions

Link to supplemental data download:

https://ugspub.nr.utah.gov/publications/reports_of_investigations/ri-290/ri-290d.pdf